Coherent Ion Acceleration using Two Electrostatic Waves

E.Y. Choueiri*and R. Spektor†
Electric Propulsion and Plasma Dynamics Laboratory (EPPDyL)
Princeton University, Princeton, New Jersey 08544

This paper is dedicated to the memory of Dr. Daniel Birx

AIAA-2000-3759‡

Abstract

We analyze a recently discovered coherent ion acceleration mechanism that relies on the nonlinear interaction of a magnetized ion with multiple electrostatic waves, at least two of which differ in frequency by an integer multiple of the cyclotron frequency. The mechanism does not require the ion to be in resonance and can accelerate an ion with an arbitrarily low initial energy, hence its basic importance to practical applications. We illustrate the fundamental features of the mechanism through a parametric numerical study of the ion's nonlinear interaction with two electrostatic waves. Compared to the wave frequencies, the wave amplitudes were found to have a weak effect on setting the energy bound of the coherent portion of the acceleration but have a strong impact on the nature of the acceleration as they control the connectivity between the coherent and stochastic domains of phase space. The lack of requirements on the initial ion energy and other fundamental properties of the mechanism point to its promise as an ion energization method for plasma propulsion.

1 Introduction

The natural phenomenon of ion acceleration transverse to the geomagnetic field by localized lower-hybrid waves in the topside ionosphere has been proposed to be the first evidence of a recently discovered ion acceleration mechanism[1]. Fundamentally, the new mechanism[2, 3] relies on the nonlinear interaction between a magnetized ion and electrostatic waves that are transverse to the magnetic field and requires that the wave spectrum contains at least two waves whose frequencies differ by an amount close to an integer multiple of the cyclotron frequency. The resulting nonlinear beating of the waves produces a slowly varying force that *coherently* accelerates the ions.

Unlike energization by resonant waves, the new mechanism does not require the ion thermal velocity to be close to the phase velocity of the wave, nor does it require that the ion velocity be above a certain threshold as in the case of the well-documented[4, 5, 6, 7, 8] energization of an ion by a *single* wave. Instead, the new mechanism can accelerate ions having arbitrarily low energies offering the potential of highly effective and adaptable means by which to effect and control the energization of ions for many applications, particularly in plasma propulsion where the efficiency of the acceleration mechanism is of prime value.

This is the first in a series of papers in which we explore this new mechanism with an eye on its application for plasma propulsion. In this first paper we will focus on describing the formalism required to study this phenomenon (Section 2), and after a review of the single-wave results (Section 3), we present a numerical study of the two-wave problem aimed at illustrating a number of the fundamental properties and complex features of the acceleration (Section 4). In subsequent papers we will explore particular aspects of the mechanism using analytical tools such as perturbation theory, evaluate more explicitly its potential for plasma propulsion and describe possible experiments to aid in this evaluation.

*Chief Scientist at EPPDyL. Assistant Professor, Applied Physics Group, MAE Department. Senior Member AIAA.
†Graduate Student, Research Assistant. Member AIAA.
‡Presented at the 36^{th} AIAA Joint Propulsion Conference, Huntsville, AL, July 16-20, 2000.

2 Hamiltonian of Motion in Action-Angle Variables

Since this is the first paper in a series of forthcoming papers on the subject and since it is a new one to the plasma propulsion community, we provide a relatively *detailed* derivation of the Hamiltonian.

Our focus is the motion of an ion in a uniform magnetic field subject to the electric field of two electrostatic waves whose wave vectors are transverse to the magnetic field. For the sake of simplicity and clarity, we follow the nomenclature of Karney[6] to derive the Hamiltonian for the case of a *single* wave then generalize the result to the case of multiple waves[2, 9].

Without loss of generality, we take the magnetic field to be along the z-axis of a cartesian coordinate system and the wave vector to be aligned with the y-axis

$$\boldsymbol{B} = B_0\hat{\boldsymbol{z}}, \qquad \phi = -\frac{E_0}{k}\sin(ky-\omega t), \tag{1}$$

where ϕ is the electrostatic potential $\boldsymbol{E} = -\nabla\phi = -\partial\phi/\partial y$ corresponding to the wave's electric field $\boldsymbol{E} = E_0\cos(ky-\omega t)\hat{\boldsymbol{y}}$ with E_0, ω and $k = 2\pi/\lambda$ denoting the wave's amplitude, frequency and wavenumber respectively. The potential energy, U, of a particle in such fields is velocity dependent and is given by[10]

$$U = q\phi - q\boldsymbol{v}\cdot\boldsymbol{A}, \tag{2}$$

where $\boldsymbol{A}$ is the magnetic potential vector ($\boldsymbol{B} = \boldsymbol{\nabla}\times\boldsymbol{A}$). The Lagrangian, L, of this system can thus be written as

$$L = \frac{m\left(\dot{x}^2+\dot{y}^2\right)}{2} + q\dot{x}A_x - q\phi, \tag{3}$$

(where the dot represents a time derivative) and can be used to define the generalized momenta p_x and p_y

$$p_x = \frac{\partial L}{\partial\dot{x}} = m\dot{x} + qA_x \tag{4}$$

$$p_y = \frac{\partial L}{\partial\dot{y}} = m\dot{y}. \tag{5}$$

with $p_z = 0$ since there is nothing to accelerate the particle along the magnetic field. The last two equations can be inverted to give

$$\dot{x} = (p_x - qA_x)/m, \qquad \dot{y} = p_y/m \tag{6}$$

which can be interpreted as the time derivatives of the conjugate generalized coordinates needed to evaluate the Hamiltonian, h, of the motion

$$h = \sum_i p_i\dot{q}_i - L. \tag{7}$$

where the summation is over the number of generalized coordinates ($i = 2$) and q_i are the generalized coordinates (to be differentiated from the ion charge q). Using Eq. (6) in the above equation, expanding and collecting terms, the resulting Hamiltonian is:

$$h = \frac{1}{2m}\left[(p_x - qA_x)^2 + p_y^2\right] + q\phi. \tag{8}$$

Noting that $A_x = -yB_o$ and using ϕ as explicitly expressed in Eq. (1), we have

$$h = \frac{1}{2m}\left[(p_x - qyB_o)^2 + p_y^2\right] - \frac{E_0}{k}\sin(ky-\omega t). \tag{9}$$

The Hamiltonian is now an explicit function of one generalized coordinate, two generalized momenta and time, i.e. $h = h(y, p_x, p_y, t)$.

We now normalize the wave frequency to the cyclotron frequency $\omega_c \equiv qB_0/m$, time to the cyclotron period $t_c = 1/\omega_c$, the coordinate to the inverse of the wavenumber, the momenta to the characteristic momentum $m\omega_c/k$ and the Hamiltonian to the characteristic energy $m\omega_c^2/k^2$ thus defining the following nondimensional parameters

$$\nu \equiv \frac{\omega}{\omega_c}, \qquad \tau \equiv \omega_c t, \qquad y' \equiv yk, \tag{10}$$

$$p_i' \equiv \frac{p_i k}{m\omega_c}, \qquad h' \equiv \frac{hk^2}{m\omega_c^2}. \tag{11}$$

In terms of these normalized parameters, the Hamiltonian $h' = (y', p_x', p_y', \tau)$ becomes

$$h' = \frac{1}{2}\left[(p_x' + y')^2 + p_y'^2\right] - \epsilon\left[\sin\left(y' - \nu\tau\right)\right] \tag{12}$$

where the non-dimensional parameter ϵ is given by

$$\epsilon = E_0\frac{qk}{m\omega^2} \tag{13}$$

and thus represents the normalized wave amplitude. It will be the primary varying parameter in the numerical investigations reported in Section 5. Note that ϵ can also be expressed as the ratio of two characteristic velocities, $(E_0/B_0)/(\omega_c/k)$.

The study of the Hamiltonian can be simplified if we can treat the time variable as any of the other generalized coordinates or momenta. In other words, we seek a canonical transformation

$$h' = h'(y', p_x', p_y', \tau) \rightarrow H = H(Q_1, Q_2, P_x, P_y). \tag{14}$$

where Q_x and Q_y are the new generalized coordinates with P_x and P_y their conjugate momenta. This can be effected by using a generating function of the "second type"[10, 11], i.e. one that mixes the old coordinate y' with the new momenta (P_x, P_y), that is $F_2 = F_2(y', P_x, P_y)$. If the following generating function is chosen

$$F_2 = (P_x - \nu\tau)x + P_y(y - \nu\tau P_x), \tag{15}$$

the canonical transformation equations

$$p'_i = \frac{\partial F_2}{\partial q'_i} \tag{16}$$

$$Q_i = \frac{\partial F_2}{\partial P_i} \tag{17}$$

$$H = h' + \frac{\partial F_2}{\partial \tau} \tag{18}$$

yield

$$Q_x = x' + p_y, \qquad , Q_y = y' + p'_x \tag{19}$$

$$P_x = p'_x + \nu\tau, \qquad P_y = p'_y \tag{20}$$

and

$$H = h' - \nu Q_x. \tag{21}$$

Therefore, as we sought, the time variable is now transformed into a generalized momentum. The new Hamiltonian resulting from this canonical transformation can thus be written as

$$H = \frac{1}{2}\left(Q_y^2 + P_y^2\right) - \nu Q_x - \epsilon \sin\left(Q_y - P_x\right). \tag{22}$$

We now seek one further transformation that will express the Hamiltonian in terms of action-angle variables[11] which provide a more natural link to the represented dynamics. For that we seek a canonical transformation

$$H = H(Q_1, Q_2, P_x, P_y) \rightarrow H = H(\psi_1, \psi_2, I_1, I_2) \tag{23}$$

where $(\psi_1, \psi_2, I_1, I_2)$ are the action-angle variables, whose physical meaning will be elucidated shortly. To effect this transformation we use a generating function of the first type, i.e. one that mixes the old coordinates Q_x, Q_y with the new ones (ψ_1, ψ_2), that is $F_1 = F_1(Q_x, Q_y, \psi_1, \psi_2)$. If we choose

$$F_1 = F_1(Q_x, Q_y, \psi_1, \psi_2) = \frac{1}{2}Q_y^2 \cot\psi_1 + Q_x\psi_2 \tag{24}$$

the corresponding canonical transformation equations

$$P_i = \frac{\partial F_1}{\partial Q_i}, \qquad I_i = -\frac{\partial F_1}{\partial \psi_i} \tag{25}$$

will yield

$$Q_x = -I_2, \qquad Q_y = (2I_1)^{1/2}\sin\psi_1, \tag{26}$$

$$P_X = \psi_2, \qquad P_y = (2I_1)^{1/2}\cos\psi_2 \tag{27}$$

and the Hamiltonian becomes

$$H = I_1 + \nu I_2 - \epsilon \sin\left[(2I_1)^{1/2}\sin\psi_1 - \psi_2\right]. \tag{28}$$

We now provide a physical interpretation of the various terms. First, the angle variable ψ_2 can be obtained directly from Hamilton's equations since the action and angle variables form a canonical set of coordinates and conjugate momenta, therefore

$$\dot{\psi}_2 = \frac{\partial H}{\partial I_2} = \nu \tag{29}$$

and $\psi_2 = \nu\tau$ takes on the physical meaning of time (multiplied by 2π) measured in units of wave periods (instead of cyclotron periods).

We note that the original Hamiltonian in Eq. (9) is explicitly independent of the x coordinate. (In the parlance of Hamiltonian mechanics, the x-coordinate is called "cyclic".) Therefore $\partial h/\partial x = 0$ and, since from Hamilton's equations $-\partial h/\partial x$ is the time derivative of the conjugate momenta p_x, we have $p_x = \alpha$ where α is a constant of the motion.

In a reference frame fixed at the guiding center of the cyclotron motion, the x-component of the velocity is linearly related to the y position by $\dot{x} = \omega_c y$, which implies that $m\dot{x} - qB_0 y = 0$ and from Eq. (4) we have $p_x = 0$. Therefore shifting our derivation to the reference frame of the guiding center corresponds to setting the constant α to zero. We do so from here on without loss of generality. By symmetry, the reference frame shift also corresponds to setting $m\dot{y} - qB_0 x = 0$ which, from the first equation in (19), gives $Q_x = 0$ which in turn leads, through Eq. (26), to $I_2 = 0$.

To find the physical meaning of the action I_1, we use Eqns. (19) and (26), to relate x' and y' to the action:

$$x' = -(2I_1)^{1/2}\sin\psi_1 \tag{30}$$

$$y' = (2I_1)^{1/2}\cos\psi_1 \tag{31}$$

which show that $x'^2 + y'^2 = 2I_1$ and as the Larmor radius (normalized by the wavenumber) ρ is equal to $(x'^2 + y'^2)^{1/2}$ we have $\rho = (2I_1)^{1/2}$. Since for a constant magnetic field the larmor radius is the ion's velocity multiplied by a constant, ρ is a measure of the velocity of the ion and the action I_1 is a measure of its *energy*.

From the last two equations we have $x' = \dot{y}' = -\rho\cos\psi_1$ and $y' = \dot{x}' = \rho\sin\psi$ which show that the angle variable ψ_1 represents the phase of the cyclotron motion.

We finally summarize the relations between all the dimensional, non-dimensional, original and transformed coordinates and momenta

$$P_y = p'_y = \frac{p_y k}{m\omega_c} = (2I_1)^{1/2}\cos\psi_1 \tag{32}$$

$$P_x = \nu\tau = \omega t = \psi_2 \tag{33}$$

$$Q_y = y' = ky = (2I_1)^{1/2}\cos\psi_1 \tag{34}$$

$$Q_x = x' + p'_y = kx + \frac{kp_y}{m\omega_c} = -I_2 = 0 \tag{35}$$

$$\rho = (2I_1)^{1/2}, \qquad \psi_1 = \tan^{-1}\frac{\dot{x}'}{x'} \tag{36}$$

The Hamiltonian can therefore be written in the following compact form

$$H = I + \epsilon\sin\left(\rho\sin\psi_1 - \nu\tau\right). \tag{37}$$

where we have dropped the subscript 1 from the action.

Further generalizing the above expression for the Hamiltonian to interactions with multiple waves is straightforward and results in the following expression

$$H = \frac{\rho^2}{2} + \sum_{i=1}^{N}\frac{\epsilon_i}{\kappa_i}\sin\left(\kappa_i\rho\sin\theta - \nu_i\tau + \phi_i\right) \tag{38}$$

where N is the number of waves, $\kappa_i \equiv k_i/k_1$, k_1 is the wavenumber of the first wave and where we have replaced ψ_1 by the symbol θ, and introduced a phase shift angle ϕ in order to make the expression more general and compatible with the formulation used in ref. [2].

3 Numerical Methods

Given initial conditions ρ_0 and θ_0, at time $\tau = 0$ we numerically integrate the differential equation of motion resulting from the Hamiltonian using the symplectic integration algorithm of ref. [12]. The method is accurate to fourth order in the time step and proved, as claimed, superior in computational efficiency and global stability to the more popular fourth-order Runge-Kutta algorithms.

The results, are plotted in two forms. The first, ρ vs τ, is essentially a time history of the ion's velocity and gives a measure of the acceleration undergone by the ion. Since much insight can be obtained by looking at the motion in phase space, the second form of data presentation is the Poincaré surface of section. Such a plot is constructed by marking on a plane, specified by setting to a constant one of the three generalized coordinates of phase space, the crossings of the particle's trajectory in phase space in a given direction across the plane's surface. Each crossing results in a dot on the Poincaré surface of section as the trajectory unfolds, and the dots can cluster in finite points, open curves or closed smooth curves for the case of *coherent* or regular motion or randomly fill an area of the cross section plane for the case of stochastic motion. The partitioning of the Poincaré surface of section into areas filled with random dots, islands where no trajectories can cross, smooth curves and speratrices provide a powerful visual analysis tool for nonlinear dynamics[11]. For our particular case, the Poincaré surface of section will be made up with the crossings of the particle's phase space trajectory with a plane whose coordinates are ρ, θ taken at a fixed $(\nu\tau)_{\mathrm{mod}\,2\pi}$.

4 Review of One-Wave Results

As mentioned in the introduction, the case of an interaction of an ion in a magnetic field with a single transverse electrostatic wave has been studied extensively using numerical calculations as well as first and second-order perturbation theories[4, 5, 6, 7, 8]. We summarize here the findings of these studies that are relevant to our discussion. There are two classes of problems in this context corresponding to 1) The *off-resonance* wave case, which means that the wave frequency is not an integer multiple of ω_c, i.e. $\nu \neq n$ and 2) the *on-resonance* wave case, where the converse is true[1].

In either case the following statement is true for the case of a single wave. *An ion can only be heated chaotically.* In other words, no coherent motion can lead to a net increase of the ion's energy irrespective of the wave's amplitude, frequency and the particle's initial conditions. Furthermore, depending on whether the wave is on or off resonance we distinguish the following features of the interaction.

Off-resonance ($\nu \neq n$)

[1] "On-resonance" here refers to the wave frequency being at or close to a cyclotron harmonic and not the phase velocity of the ion.

- Chaotic dynamics can only occur if the wave's amplitude is above a certain threshold given by

$$\epsilon_{th} \simeq \frac{\nu^{3/4}}{4} \tag{39}$$

- For $\epsilon > \epsilon_{th}$, the chaotic domain is only accessible if the initial ion normalized Larmor radius[2] (or velocity) is above a lower bound given by

$$\rho^* \simeq \nu - (\epsilon)^{1/2}. \tag{40}$$

  This means that an ion whose initial energy is below that corresponding to this threshold, will not receive a net acceleration by the wave, since it will not reach the chaotic domain. Note that an increase in amplitude will decrease the threshold, therefore for a sufficiently high wave amplitude, an ion's motion can be made chaotic. This is also intuitive.

- The chaotic domain has also an upper bound ρ_{ub},

$$\rho_{ub} \simeq \left(\frac{2}{\pi}\right)^{1/3} (4\epsilon\nu)^{2/3}. \tag{41}$$

  If an ion is above that threshold its dynamics will not be chaotic even if the wave energy is above ϵ_{th} and thus cannot be accelerated.

On-resonance ($\nu = n$)

- Instead of a purely stochastic region in phase space there is a web structure in which stochastic regions connect regular trajectories. This web structure is not strictly bounded on the high ion energy side but becomes thinner at high energies.

- Like the stochastic region of the off-resonance case, this web structure also has a lower bound on ρ_0 given essentially by Eq. (40) when ν is sufficiently large.

- At lower values of ν, however, the bound takes on a form that has a far more complicated dependence on ν and ϵ[8] but has the essential feature that, unlike in Eq. (40), it *increases* with increasing energy. This leads to the counter-intuitive result that by *decreasing* the wave's amplitude an ion's motion can be made to become chaotic.

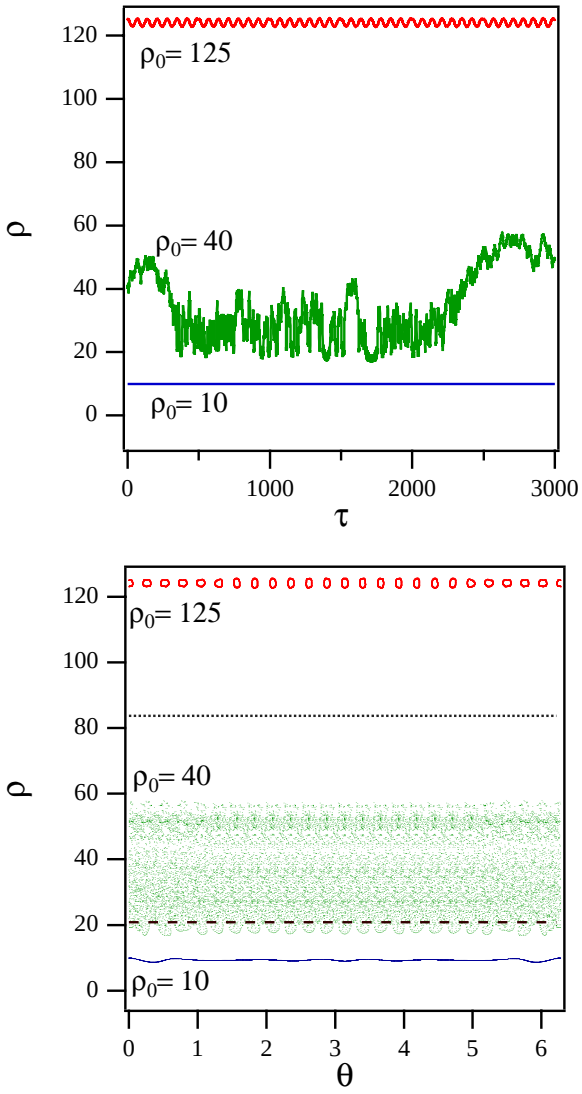

Figure 1: Acceleration history and Poincaré surface of section for three cases of an ion interacting with a single wave having $\nu = 24$, $\epsilon = 10$. The initial conditions ρ_0 for the ions are marked on the plots and $\theta_0 = 0$ for all three cases. The dashed (lower) and dotted (upper) horizontal lines denote the values of ρ^* and ρ_{ub} given by Eqs. (40) and (41) respectively.

[2]The Larmor radius is actually a measure of the ion's velocity. Since ρ is uniquely related to the action I it is sometimes talked of as being an index of the energy.

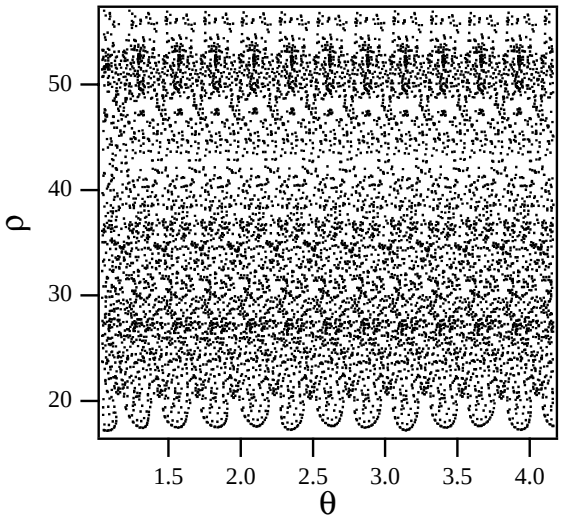

Figure 2: Close up on the Poincaré surface of section of Fig. (1) showing the web structure.

We now illustrate some of these features with a numerical study of an ion interacting with a single wave. Since our two-wave study will focus on on-resonance waves, we consider here also an on-resonance wave with $\nu = 24$ and $\epsilon = 10$. We calculate the motion for three test ions ($\theta_0 = 0$). The first is chosen with $\rho_0 = 10$, that is an initial energy that is below that required by Eq. (40) and therefore we should expect the ion's motion to be regular without any acceleration by the wave. This is indeed the case as can be seen from both plots in Fig. (1).

The ion with the highest initial energy was chosen with $\rho_0 = 125$ so that it is above the upper threshold given by Eq. (41). The evolution of its subsequent Larmor radius in time shows no net change in energy. On the Poincaré surface of section, the phase space trajectory leaves small circular "islands" which are visited alternatively in time. These islands are centered around $\rho = \rho_0$. The ion with the intermediate initial energy ($\rho_0 = 40$) shows a net increase in energy. Its signature in the Poincaré surface of section shows an intricate web of interconnecting areas of stochasticity and regular motion as mentioned in the discussion above. This web is shown in more detail in the close-up plot of Fig. (2).

It is interesting to note from Fig. (1) that the web extends a little below ρ^* as given by Eq. (40) and denoted by a dashed horizontal line on that plot.

5 Interaction with Two Waves

We now proceed to our numerical study of the interaction of a magnetized ion with two waves and illustrate some striking differences with the previous single-wave results.

The fundamental effect occurs when at least two waves are present having frequencies that differ from each other by an integer number times the cyclotron frequency[2]. In the following we present a numerical study that will bring forth some of the fundamental aspects of this nonlinear interaction. We will postpone to another paper our attempts to explain the results analytically and instead limit ourselves to a phenomenological discussion based on the results of the numerical simulations.

5.1 Parameters

We choose the wave amplitude ϵ as the primary varying parameter for our study because we see from the Hamiltonian, Eq. (38), that it is ϵ that scales the degree of coupling between the two harmonic oscillators (the cyclotron motion and the wave motion) and consequently we expect it to have a strong effect on the character of the motion. Furthermore, since the largest acceleration in previous studies[2] was found to occur when the two waves have the same amplitude, we set $\epsilon_1 = \epsilon_2 = \epsilon$. We also choose two on-resonance waves whose normalized frequencies ν_1 and ν_2 differ by 1. We choose ν_1 to be large enough that we can expect the boundary conditions discussed in the previous section approximately hold but small enough that we may expect some interesting departures. Specifically, we take $\nu_1 = 24$ and $\nu_2 = 25$. Finally, we start all the ions we consider from the initial conditions $\rho_0 = 1$ and $\theta_0 = 0$ and set the wave phase shifts $\phi_1 = \phi_2 = 0$.

5.2 Coherent Acceleration and Connection to Stochastic Domain

We immediately see from Fig. (3) the primary feature that the ion, although starting well below the chaotic domain, picks up energy steadily and accelerates coherently exceeding the bound ρ^*. For each of the time traces, we note a steady acceleration mode followed by a fluctuating mode in which the ion velocity fluctuates widely reaching values as high as two orders of magnitudes larger than the initial velocity. The two modes are also differentiated by their disparate time scales. Increasing the wave amplitudes greatly

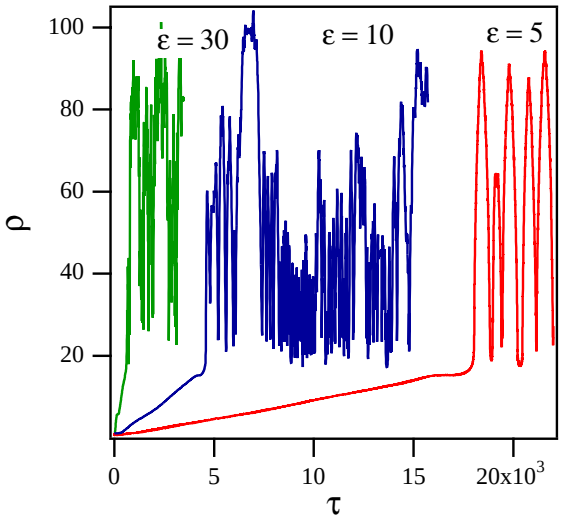

Figure 3: Motion history at three different wave amplitudes, $\epsilon = 5, 10$ and 30. With $\nu_1 = 24$, $\nu_2 = 25$, $\kappa = 1$, $\phi_1 = \phi_2 = 0$, and the initial conditions $\rho_0 = 1$ and $\theta_0 = 0$.

enhances the acceleration. Specifically, we note from the plots that that the acceleration time scales inversely with the square of the wave amplitudes. All ions, however, accelerate coherently up to roughly the same energy level before entering the chaotic domain. This coherent acceleration from an arbitrarily low energy is *impossible* in the case of an interaction with a single wave.

The character of this motion can be further elucidated from the Poincaré sections shown in Fig. (4) From these plots we note the fundamental feature that *the coherent and stochastic parts of phase space are connected* and the orbit of an ion can take it from one domain to the other. This is in complete contrast to the single-wave case we illustrated in Fig. (1).

On all Poincaré section plots, the dashed (lower) and dotted (upper) horizontal lines denote the values of ρ^* and ρ_{ub} given by Eqs. (40) and (41) respectively calculated with the lower of the the two frequencies[2].

We see that for the low wave amplitude, $\epsilon = 5$, the ion reaches the edge of the coherent domain and enters a domain that is not completely stochastic, but rather, in a manner reminiscent of the web structure

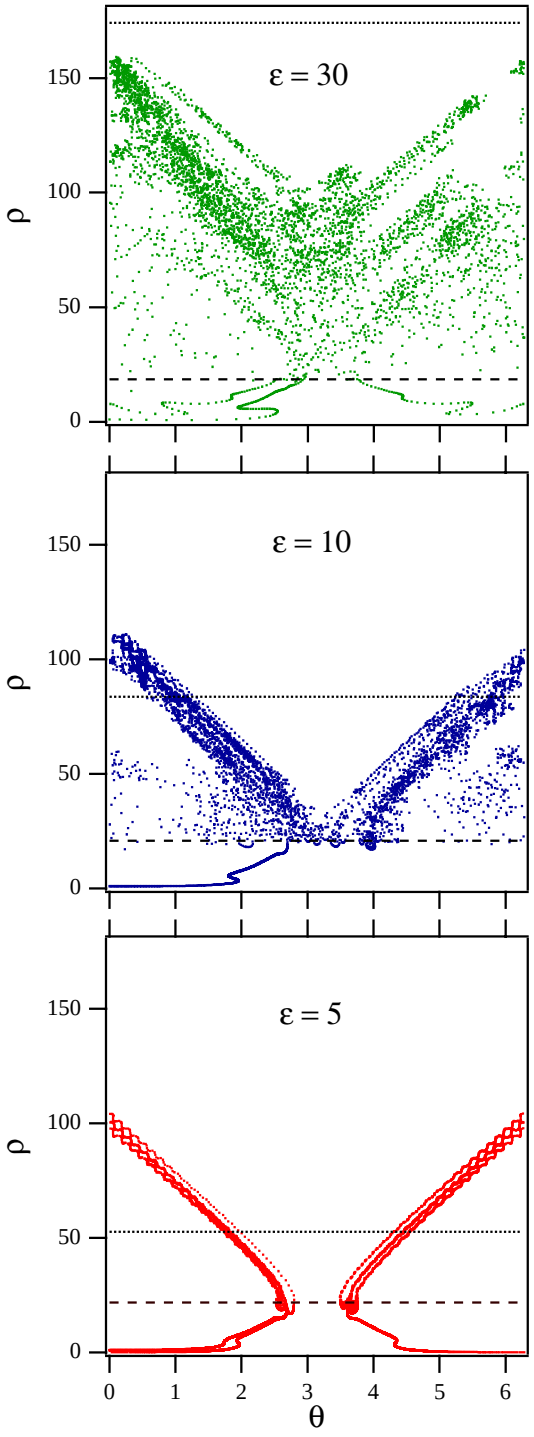

Figure 4: Poincaré sections corresponding to the three cases shown in Fig. (3).

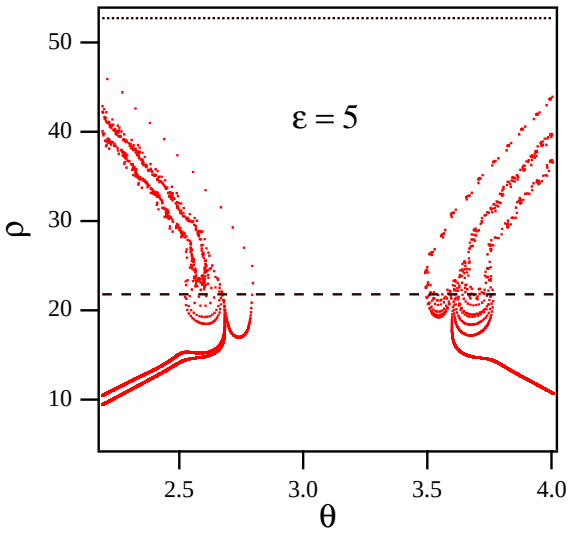

Figure 5: Close up of the Poincaré section at the bottom of the previous figure.

of Fig. (2), consists of webs of stochasticity relating essentially coherent orbits. A close up of that intricate structure is shown in Fig. (5). From the corresponding motion history in Fig. (3), this type of motion can be seen to be characterized by quasi-periodic excursions into the high ρ part of the ion energy range followed by quick deceleration to energies near those corresponding to ρ^*.

As the wave amplitude is further increased, these webs of stochasticity quickly enlarge to engulf any vestiges of coherence in regions above ρ^* as can be seen from the top two plots of Fig. (4).

It is apparent from these plots that the connection between the coherent and stochastic domains is not uni-directional, i.e. just as a particle in coherent motion can be accelerated to the stochastic realm, a particle in stochastic motion can fall into the coherent range when it reaches the lower boundary with the appropriate conditions. Had the traces shown in Fig. (3) not been truncated (in time) for the display, randomly distributed excursions of the particle orbits between the stochastic and coherent domains would have been apparent. The smooth curves on both sides of $\theta = \pi$ at the bottom part of the plots in Fig. (4) are the Poincaré section signatures of the these excursions.

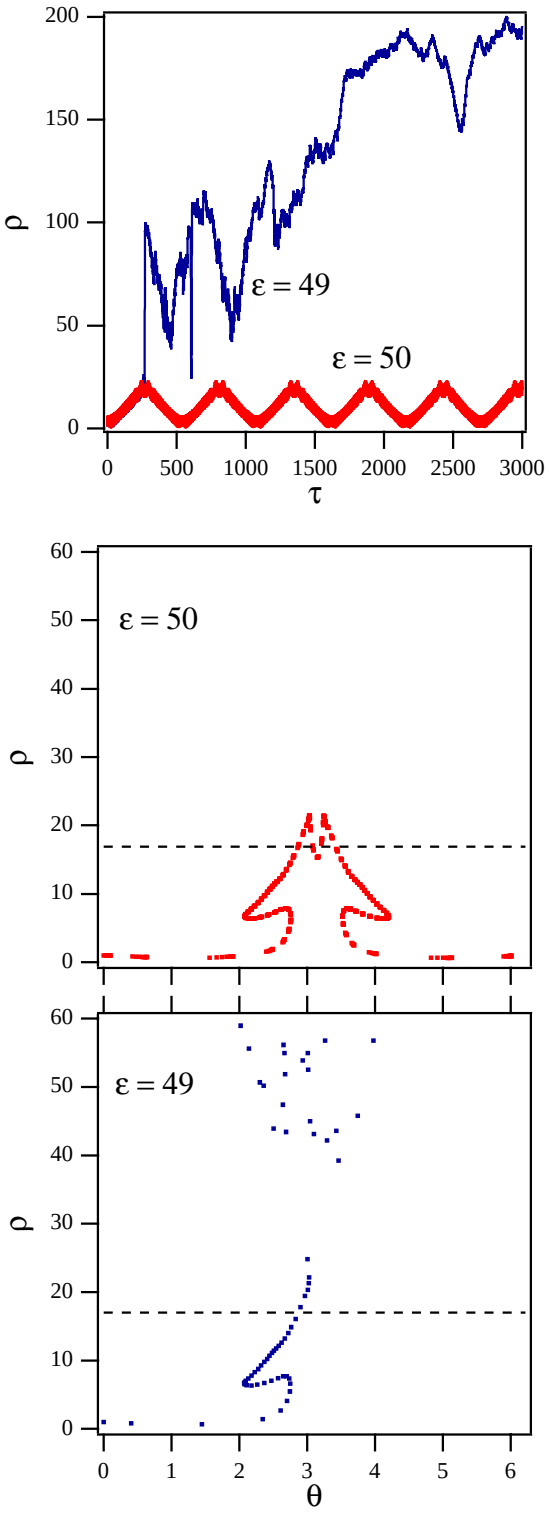

Figure 6: Motion histories and Poincaré sections for $\epsilon = 49$ and $\epsilon = 50$. Other parameters are the same as those for Fig. (3).

5.3 Stochastic Domain Inaccessibility

If we further increase the amplitude of the waves we eventually come to a condition where the stochastic part of phase space becomes suddenly inaccessible. This "locking" of stochastic phase space happens at a certain threshold in ϵ as illustrated in Fig. (6). As ϵ in that figure is raised from 49 to 50, the ion is effectively locked out of stochastic phase space and its energy oscillates bounded by ρ^*. While the ion in the higher amplitude wave attains on the average a velocity half as high as that corresponding to ρ^*, an ion in a wave having an amplitude just below this threshold, can "escape" to the stochastic domain and may be accelerated to significantly higher energies as shown in that plot.

This sudden inaccessibility to the stochastic realm, may be related to a raising of the effective lower bound of the stochastic region with the wave amplitude which is reminiscent of the effect discussed in the previous section in the context of an interaction with the on-resonance single wave. While an analytical method for calculating that lower boundary has been developed using second-order Lie perturbation theory[8], it is strictly valid for an interaction with a single wave. One would expect, however, that for the two-wave case, this phenomenon is also related to a raising of this boundary with wave amplitude to levels just above those attained by coherent acceleration.

The difference between these two levels however, seems to remain small as implicitly implied by the results shown in Fig. (7), where we see in the top two panels that a further increase in the amplitude of the waves above the inaccessibility threshold, leads to a "re-opening" of the stochastic part of phase-space. This re-accessibility, for a given set of conditions, occurs at a time τ which decreases with wave amplitude as indicated by the two cases shown in Fig. (7) for $\epsilon = 75$ and $\epsilon = 80$.

It is also interesting to note from the motion histories shown in Fig. (3) and the top panels of Figs. (6) and (7) that a certain level of periodicity develops in the coherent part of the motion as the wave amplitude is increased. This is reflected in the apparent thickening of the part of the curves that corresponds to coherent motion. This thickening, when viewed on a finer time scale, is essentially an increase in the periodic structure of the motion history curve which corresponds to progressive tightening, with increasing ϵ, of the mushroom-like structure in the coherent parts of Poincaré sections. This is seen clearly in Fig. (8) where we show the superimposed Poincaré sections for the coherent parts of the ion orbits for

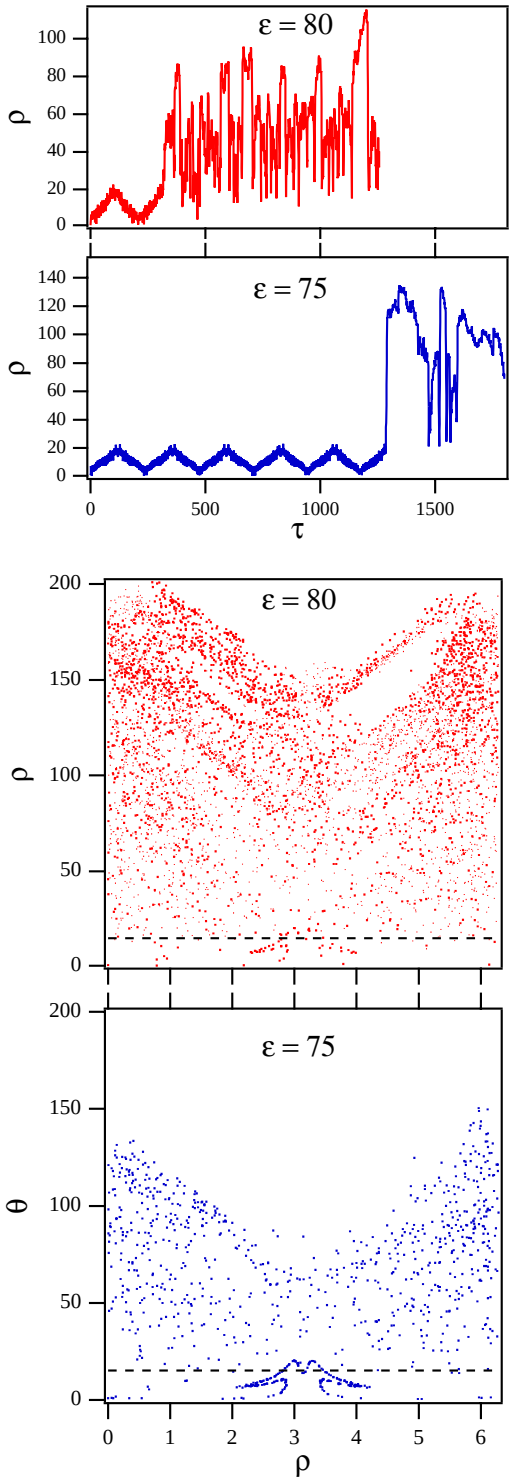

Figure 7: Motion histories and Poincaré sections for $\epsilon = 75$ and $\epsilon = 80$. Other parameters are the same as those for Fig. (3).

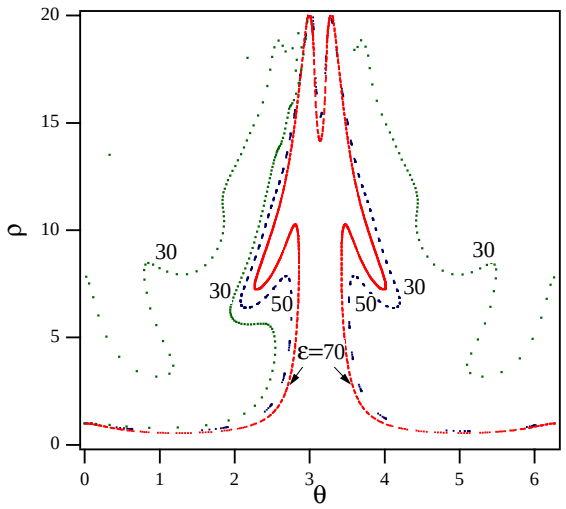

Figure 8: Superimposed Poincaré sections for the coherent parts of the ion orbits for the three cases corresponding to $\epsilon = 30, 50$ and 70.

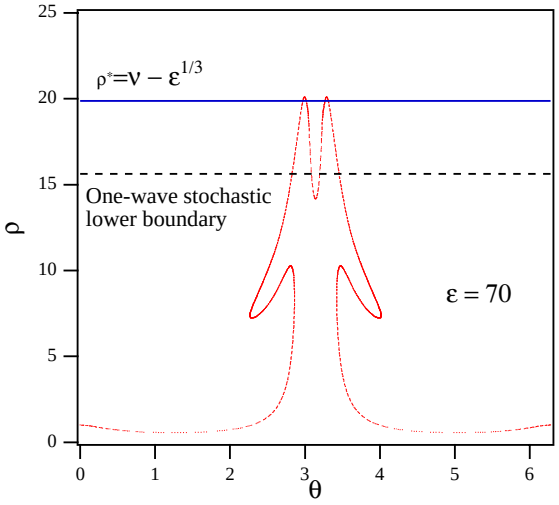

Figure 9: Poincaré section for the coherent part of the ion orbit for $\epsilon = 70$ which corresponds to a case where the stochastic regime remains inaccessible, until a later time. The lower dashed line shows the boundary predicted by Eq. (40) and the solid line shows the empirical model given by Eq. (42)

the three cases corresponding to $\epsilon = 30, 50$ and 70. As the wave amplitude is increased, the ion enters the stochastic domain (or exits it, or is reflected by its lower boundary) at a cyclotron phase angle progressively closer to π. In this sense the accessibility to stochasticity becomes limited to ions with θ near π.

5.4 Lower Boundary of Stochasticity

We note that although the lower boundary of the stochastic domain, given by Eq. (40), is roughly in agreement with the calculated boundary as seen from the Poincaré sections of the previous figures, it can differ by more than 20% for the conditions we studied. Specifically, at and moderately above the values of ϵ for which the stochastic region becomes largely inaccessible, the boundary predicted by Eq. (40) is noticeably below the actual limit as defined by the maximum value that ρ acquires *coherently* in the Poincaré section. This is illustrated in Fig. (9) for $\epsilon = 70$ which corresponds to a case where the stochastic regime remains inaccessible, until a later time. Unlike in the case where the coherent and stochastic domain are connected, the numerical determination of the boundary becomes unambiguous in the case where the stochastic region becomes largely inaccessible, since then the coherent orbit on the Poincaré section has an effective upper bound in ρ. For these conditions we found, by conducting a number of numerical simulations, that the following "empirical" model better fits the results

$$\rho^* = \nu - \epsilon^{1/3}. \tag{42}$$

The extent of agreement of both Eq. (40) and Eq. (42) with the numerically determined boundary for six cases with differing values of ν and ϵ, is shown in Fig. (10). It is clear form the plot that both predictions are equally good at large ρ^* (i.e. large ν or small ϵ) but the empirical model is better at lower wave frequencies.

6 Conclusions

After an explicit derivation of the Hamiltonian for a magnetized particle interacting with multiple waves transverse to the magnetic field, and a review of the well-documented one-wave case, we focused on the case of two waves as a more manageable illustration of the fundamental features of the recently discovered[2, 3] ion mechanism by multiple waves. The mechanism relies on the nonlinear interaction of a magnetized ion with multiple electrostatic waves, at least two of

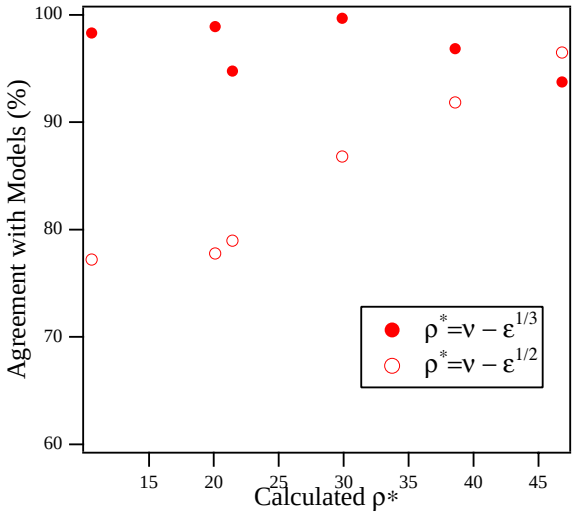

Figure 10: Extent of agreement of Eq. (40) and Eq. (42) with the calculated value of the boundary ρ^*.

which differ in frequency by an integer multiple of the cyclotron frequency. The resulting rich dynamics were illustrated through numerical "experiments" in which the amplitude of the two waves was the varying parameter. The following fundamental features were noted:

1. An ion, arbitrarily below the (stochastic) energization threshold required for single-wave acceleration, can pick up energy steadily and accelerate coherently.

2. The coherent and stochastic motion domains in phase space are connected unlike in the case of an interaction with a single wave.

3. Depending on the amplitude and frequency of the waves and the ion initial conditions, the ion can accelerate through the low energy boundary of the stochastic domain and be energized further stochastically.

4. The coherent acceleration time scales inversely with the square of the wave amplitudes.

5. At low enough wave amplitudes, the motion of the ion above the single-wave stochastic boundary, is not purely stochastic but rather constitutes of motion along coherent orbits connected in phase space by regions of stochasticity. As the wave amplitude is increased, these stochastic webs engulf the coherent orbits above the stochastic low energy boundary but the acceleration below that boundary remains coherent.

6. At a certain wave amplitude, the stochastic domain becomes inaccessible and the ion undergoes successive coherent acceleration and deceleration cycles (maintaining on the average a velocity half as high as that corresponding to the boundary) until conditions favoring its reentry into the stochastic domain become available. These conditions include a higher wave amplitude and/or a longer time period through which the ion can eventually visit dynamical states that allow accessibility.

7. At least for conditions where the stochastic domain is not readily accessible, the highest velocity the ion acquires does not scale according to the one-wave stochastic boundary limit i.e. $\rho^* \simeq \nu - \epsilon^{1/2}$. For the cases we studied, an empirical scaling was found to be $\rho^* \simeq \nu - \epsilon^{1/3}$.

8. With increasing wave amplitude, the ion's coherent motion acquires a periodic modulation and the accessibility to stochasticity becomes limited to ions with a narrow distribution of cyclotron phase angles.

This fundamental understanding paves the way for future analytical and experimental studies of the mechanism and the evaluation of its potential for plasma propulsion applications.

References

[1] K. Ram, A. Bers, and D. Benisti. Ionospheric ion acceleration by multiple electrostatic waves. *Geophysical Research Letters*, 103:9431–9440, 1998.

[2] D. Benisti, A.K. Ram, and A. Bers. Ion dynamcis in multiple electrostatic waves in a magnetized plasma, I. Coherent acceleration. *Physics of Plasmas*, 5(9):3224–3232, 1998.

[3] D. Benisti, A.K. Ram, and A. Bers. Ion dynamcis in multiple electrostatic waves in a magnetized plasmai, II. Enhancement of the acceleration. *Physics of Plasmas*, 5(9):3233–3241, 1998.

[4] C.F.F. Karney and A. Bers. Stochastic ion heating by a perpendicularly propagating electro-

static wave. *Physical Review Letters*, 39:550, 1977.

[5] A. Fukuyama, H. Mometa, R. Itatani, and T. Takizuka. Stochastic acceleration by an electrostatic wave near ion cyclotron harmonics. *Physical Review Letters*, 38:701, 1977.

[6] C.F.F. Karney. Stochastic ion heating by a lower hybrid wave. *Physics of Fluids*, 21(9):1584–1599, 1978.

[7] G.M. Zaslavsky, R.Z. Sagdeev, D.A. Usikov, and A.A. Chernikov. *Weak Chaos and Quasi-Regular Patterns*. Cambridge University Press, Cambridge, 1991.

[8] A.K. Ram D. Benisti and A. Bers. Lower bound in energy for chaotic dynamics of ions. *Physical Letters A*, 233:209, 1997.

[9] P. Chia, L. Schmitz, and R.W. Conn. Stochastic ion behavior in subharmonic and superharmonic electrostatic waves. *Physics of Plasmas*, 3(5):1545–1568, 1996.

[10] H. Goldstein. *Classical Mechanics*. Addison-Wesley, Cambridge, MA, 1951.

[11] A.J. Lichtenberg and M.A. Lieberman. *Regular and Chaotic Motion*. Addison-Wesley, Cambridge, MA, 1983.

[12] J. Candy and W. Rozmus. A symplectic integration algorithm for separable hamiltonian functions. *Journal of Computational Physics*, 92:230–256, 1991.